Emergence of scaling associated with complex branched wave structures in optical medium

Xuan Ni, Ying-Cheng Lai, and Wen-Xu Wang

Citation: Chaos 22, 043116 (2012); doi: 10.1063/1.4766757
View online: http://dx.doi.org/10.1063/1.4766757
View Table of Contents: http://chaos.aip.org/resource/1/CHAOEH/v22/i4
Published by the American Institute of Physics.

Emergence of scaling associated with complex branched wave structures in optical medium

Xuan Ni,[1] Ying-Cheng Lai,[1,2] and Wen-Xu Wang[1,3]
[1]*School of Electrical, Computer and Energy Engineering, Arizona State University, Tempe, Arizona 85287, USA*
[2]*Department of Physics, Arizona State University, Tempe, Arizona 85287, USA*
[3]*Department of Systems Science, School of Management and Center for Complexity Research, Beijing Normal University, Beijing 100875, China*

(Received 27 July 2012; accepted 22 October 2012; published online 26 November 2012)

Branched wave structures, an unconventional wave propagation pattern, can arise in random media. Experimental evidence has accumulated, revealing the occurrence of these waves in systems ranging from microwave and optical systems to solid-state devices. Experiments have also established the universal feature that the wave-intensity statistics deviate from Gaussian and typically possess a long-tail distribution, implying the existence of spatially localized regions with extraordinarily high intensity concentration ("hot" spots). Despite previous efforts, the origin of branched wave pattern is currently an issue of debate. Recently, we proposed a "minimal" model of wave propagation and scattering in optical media, taking into account the essential physics for generating robust branched flows: (1) a finite-size medium for linear wave propagation and (2) random scatterers whose refractive indices deviate continuously from that of the background medium. Here we provide extensive numerical evidence and a comprehensive analytic treatment of the scaling behavior to establish that branched wave patterns can emerge as a general phenomenon in wide parameter regime in between the weak-scattering limit and Anderson localization. The basic physical mechanisms to form branched waves are breakup of waves by a single scatterer and constructive interference of broken waves from multiple scatterers. Despite simplicity of our model, analysis of the scattering field naturally yields an algebraic (power-law) statistic in the high wave-intensity distribution, indicating that our model is able to capture the generic physical origin of these special wave patterns. The insights so obtained can be used to better understand the origin of complex extreme wave patterns, whose occurrences can have significant impact on the performance of the underlying physical systems or devices. [http://dx.doi.org/10.1063/1.4766757]

Complex wave phenomena occur in many fields of science and engineering. Branched, fractal-like wave patterns arise in diverse areas such as oceanography, acoustics, optics, and solid-state devices. Weather such wave structures possess a generic physical origin is a matter of active debate. For example, it was thought previously that nonlinearity in the physical medium supporting wave propagation is essential, but recent experimental evidence indicated that branched wave patterns can arise even in the absence of nonlinearity. It is thus of general interest to develop a minimal model containing the most essential physics to account for the emergence of branched wave structures. A quantitative measure of the validity of such a model is its ability to predict an experimentally widely observed, universal feature of branched wave structures: non-Gaussian statistics of wave intensity with an algebraic tail in the probability density function. The aim of this paper is to analyze a minimal model that we recently proposed to understand the emergence and statistical scaling properties of robust complex branched wave patterns in optical media. Our model contains two basic physical ingredients: (1) a uniform medium of finite size and (2) spatially localized scatterers randomly distributed in the medium, the refractive indices of which deviate from that of the background medium. The second ingredient is required for generating dynamics beyond simple linear wave propagation. We present a comprehensive analytic treatment of the model to establish that (1) qualitatively, it can generate robust branched, fractal-like wave patterns and (2) quantitatively, the model leads naturally to an algebraic, long-tail type of distribution in the wave intensities. We expect the physical insights gained here can be useful for understanding complex wave phenomena in general.

I. INTRODUCTION

When waves propagate through random media, extreme events and complex structures such as rogue waves and branched, fractal-like wave patterns can form. There has been a substantial amount of interest in complex wave phenomena due to their occurrences in a host of physical systems. For example, in oceanography, rogue waves are an issue of great concern. In the past fifteen years or so there had been experimental and theoretical studies of rogue waves arising from long-range acoustic wave propagation through ocean's sound channel,[1,2] as well as large-scale experiments on directional ocean waves to probe the physical and dynamical origin of these extreme waves.[3] Extreme

events and complex wave patterns have also been identified in many other physical situations such as light propagation in doped fibers,[4,5] acoustic turbulence in superfluid helium,[6] resonances in nonlinear optical cavities,[7] linear light-wave propagation in multi-mode glass fiber,[8] and electronic transport in semiconductor two-dimensional electron gas (2DEG) systems.[9] Despite previous efforts, an accepted, relatively complete understanding of complex extreme waves at the level of fundamental physics is still lacking.

To illustrate the extent to which complex branched wave patterns are presently understood, we choose electronic transport in 2DEG systems as an example. In Ref. 9, electron flows from a quantum point contact were reported to exhibit a striking, branched or fractal-like behavior with highly non-uniform amplitude distribution in the physical space. The observed separate, narrow strands of greatly enhanced electron wave intensities were argued to be caused by random background potentials and quantum coherent phase interference among the electron wave functions. Subsequently a theory was proposed[10] to predict the statistical distribution of the intensities of branched electron flows in the presence of weak, correlated Gaussian random potentials.

The generic origin of wave branching behavior is a matter of active debate.[11] A tacit assumption in most previous investigations is nonlinearity in the underlying medium. In particular, it had been believed that the existence of many uncorrelated, spatially randomly distributed wave elements is key to the occurrence of these exotic wave patterns. These elements can be, for example, solitons in nonlinear systems. However, quite recently, it was demonstrated experimentally in a microwave system[12] and in a multi-mode optical fiber[8] that branched wave patterns can occur even in the absence of nonlinearity. In fact, in the latter case, granularity of light speckles at the fiber exit and inhomogeneity in the spatial clustering of the speckle patterns are speculated to be the two ingredients that trigger complex wave patterns. These recent works thus demonstrate that nonlinearity is not absolutely essential for the emergence of these extreme waves. A question of significant theoretical and experimental interest concerns thus about a minimal physical model that can generate robust branched wave patterns, so that their generic and physical origin may be elucidated. A related issue concerns the statistical properties of these waves. In this regard, a general observation in all contexts where branched wave structures arise is the non-Gaussian statistics of the wave amplitude. Typically there is a long tail in the probability density function, which characterizes the extreme intensity of the waves. An essential requirement for a valid minimal model of branched wave patterns is thus that it should generate the universally observed long-tail distribution in the wave intensity.

In a recent brief note,[13] we proposed a class of minimal models for branched wave patterns in the context of wave propagation in two-dimensional optical medium. The model contains two basic physical elements: (1) a uniform medium of finite size and (2) spatially localized scatterers randomly distributed in the medium, the refractive indices of which deviate from that of the background medium. The deviations can occur in both ways which, in the case of negative deviation, may correspond to scatterers that are effectively negative-indexed, or *metamaterials*. The second element is required for generating dynamics beyond simple linear wave propagation. We have demonstrated that such a minimal model can generate robust branched wave patterns, regardless of the detailed distribution of the refractive-index deviations associated with the random scatterers. The purposes of this paper are twofold: (1) to provide extensive numerical evidence for the emergence of branched wave patterns and (2) to present a comprehensive analytic treatment of the minimal model by focusing on the theoretical derivation of the power-law type of long-tail distribution in the wave intensities.

More specifically, the model, approach, and findings of our study can be stated as follows. We consider the setting where a polarized monochromatic light propagates in a dielectric optical medium with structural imperfections characterized by random refractive-index disorders (scatterers) of size comparable to the wavelength. Our numerical scheme employs the standard finite-difference frequency-domain (FDFD) method[14–17] to calculate the intensity of the scattered field through multiple scatterers. In the weak scattering limit, i.e., when the wavelength λ is much smaller than the mean free path l, we obtain striking branching flow structures of propagating light, similar to those observed in the 2DEG and microwave transport experiments. As the spatial density of the scatterers is increased, the intensity patterns exhibit more pronounced fractal-like behavior, where branches of extraordinarily high intensities tend to enhance themselves when forking into narrower and even smaller paths. Anderson localization of light is also observed as the mean free path approaches the strong scattering limit ($l \sim \lambda$). Our extensive numerical computation also confirms that the branched structure can result from the caustics of the flow rather than the valleys of the random scatterers. We find that branched waves generically arise in the regime between weak scattering and strong localization of light waves.

In order to obtain a comprehensive understanding of the occurrence of branched waves in optical media and also to uncover their statistics, we develop a detailed analytic theory. Utilizing the Green's function method, we treat the scattering of two-dimensional polarized light wave off a single scatterer and obtain a theoretical explanation for the reason why the wavelength needs to be comparable to the size of the scatterer in order for noticeable large fluctuations of branching strands to be observed. In contrast to the existing theory[10] which deals with stretches and folds in classical ray dynamics in a concrete and somewhat abstract manner, our theory enables us to *visualize* the branching flow structures of the scattered light intensities in different angular directions. Based on the results from scattering off a single scatterer, we next extend our treatment to multiple scatterers. In this case, coherent backscattering and recurrent multiple scattering become important, and they together contribute dominantly to the formation of extremely large amplitude events. This unstable branch stretching and accumulation process is highly sensitive to the scatterers' spatial

distribution and thus is critical to the formation of fractal-like wave patterns. Because of the large intensity fluctuations caused by wave interference and the complexity of random-scatterer configuration, it is essential to focus on the statistical distribution function of light intensities. We have succeeded in deriving a formula for the distribution function of high intensities, which follows an algebraic (power-law) scaling law in the weak-scattering limit. This means that, associated with the branched waves, there are points in the space at which exceedingly large intensities can arise, the "hot" spots, in contrast to situations governed by Gaussian type of intensity distributions.[18–21] Note that the algebraic distribution was previously observed in electronic transport in 2DEG systems.[10] In the optical media, however, away from the weak-scattering limit (e.g., $\lambda/l \sim 0.35$), our theory predicts a small deviation from the algebraic scaling law, but the overall distribution is still markedly long-tailed.

In Sec. II, we describe our model and present extensive numerical evidence of branched wave patterns in optical media with negative- and positive-index disorders, and a mixture of both. In Sec. III, we develop a detailed analytic theory based on electromagnetic wave scattering to uncover the physical origin underlying the emergence of branched wave structures. The theory allows us to predict the significant statistical behaviors of these complex wave patterns, which are verified numerically. Conclusions and discussions are presented in Sec. IV.

II. NUMERICAL RESULTS

We consider a polarized, monochromatic, Gaussian light beam propagating in a dielectric medium of refractive index n_0, where the medium has embedded within itself N random scatterers. The spatial distribution function of the refractive index for the whole system can be written as

$$n(\mathbf{r}) = n_0 + \sum_{i=1}^{N} \Delta n_i \exp[-|\mathbf{r} - \mathbf{r}_i|^2/(2\sigma^2)], \qquad (1)$$

where Δn_i is the magnitude of the refractive index of the ith scatterer relative to that of the medium, and $\mathbf{r} = (x, y)$ is a two-dimensional vector. Each scatterer is characterized by a Gaussian-shaped refractive index profile, whose effective radius is σ. To simulate the scattering of electromagnetic waves, we use the standard FDFD method.[17] The wavelength is chosen to be $\lambda = 1\ \mu$m so that the scattering strength ratio is $\lambda/l \sim 0.35$. Figures 1(a)–1(d) show, for a rectangular medium of size $35\ \mu\text{m} \times 70\ \mu\text{m}$ and $N = 300$, four typical cases of the distribution of the scattering field strength, where the scatterers have negative refractive-index variations ($\Delta n_i < 0$) for panels (a),(b), and positive variation ($\Delta n_i > 0$) for panel (c), and a mixed distribution of negative and positive variations for panel (d). Signatures of branched wave patterns, especially a fractal-like branching structure, are apparent in all cases. Numerically, we observe that the shape of the refractive-index distribution associated with the random scatterers does not have a significant effect on the emergence and the statistical properties of the branched wave structures. However, in order to preserve high numerical accuracy and reduce artificial reflection effect, we have chosen some smoothly varied shape, such as the Gaussian shape. As will be derived analytically, in order to observe sharp, narrow, branch-like flows, the sizes of the scatterers should be comparable to the wavelength λ. Note that the wave patterns for the negative and positive variation cases exhibit somewhat different branched forking structures. This is largely due to the fact that higher refractive-index regions attract light rays while lower refractive-index regions repel them. In the short-wavelength limit, the negative-indexed scatterers are equivalent to repulsive potential hills, while the positive ones are effectively attractive potential wells for light rays. In both cases, chaos can arise in the zero wavelength limit.

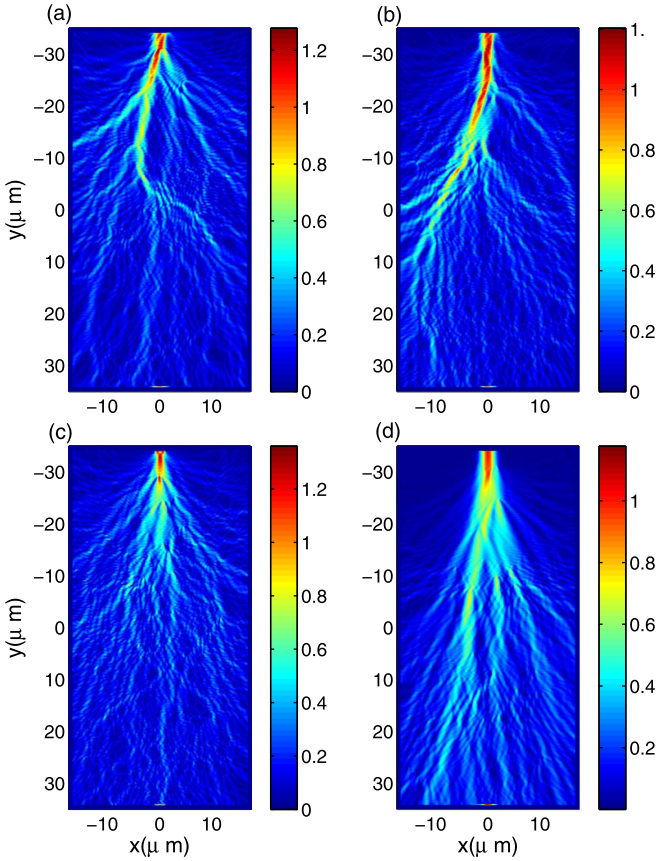

FIG. 1. For a rectangular optical medium of size $35\mu\text{m} \times 70\mu\text{m}$ with $N = 300$ spatially localized, Gaussian-shaped scatterers, typical spatial distributions of the magnetic field strength $|H|$ of the scattered waves. In each case, an external polarized, monochromatic, Gaussian wave of width $w = 1\mu$m and unit intensity is sent from the top of the region. For panels (a) and (b), the refractive-index variations are negative: $\Delta n_i = -0.5$. The variation is positive for panel (c): $\Delta n_i = 0.5$. For panel (d), Δn_i is randomly selected from the range [–0.5, 0.5]. Other parameters are the same for all panels: $n_0 = 1$, $\lambda = 1\mu$m, and $\sigma = 0.22$. We observe signatures of branched, fractal-like wave patterns in all cases.

Figure 2 shows the positions of the random scatterers superimposed on top of the branched wave pattern. A feature typical of the observed fractal-like wave patterns is that the wave branches tend to pass along the sides of the scatterers instead of going through the smooth valleys among the scatterers. This feature appears to be shared by electronic branched wave patterns in 2DEG systems,[9,10] where it was suggested that the wave branches may result from caustics in the corresponding classical regime. As for 2DEG systems,

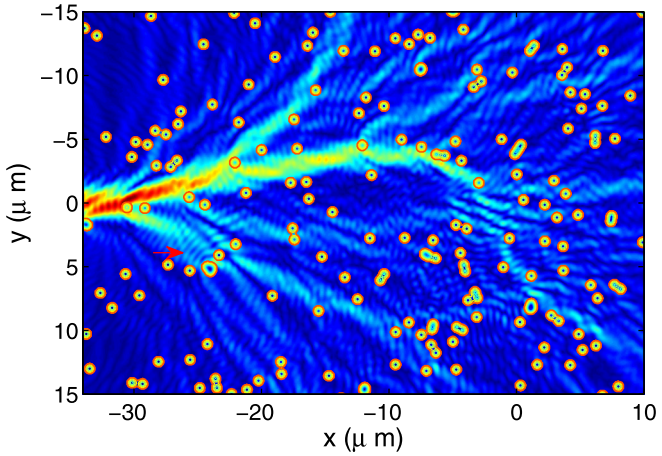

FIG. 2. Positions of scatterers (marked by red circles) on top of various wave paths. Intensive wave branches tend to go through various boundaries of scatterers instead of passing through the various smooth valleys in between. Red arrow marks the position where interference fringes are observed.

we also observe fringe patterns (e.g., marked by a red arrow in Fig. 2), which are separated in space by about $\lambda/2$. It is known that coherent backscattering[22] of light by disorders is responsible for the formation of these fringe patterns. More specifically, light backscattered by the disorders (in Fig. 2, close to the arrow along the propagating direction of light) tends to interfere with the forward propagating light, giving rise to the fringes separated by half-wavelength.

To gain more physical insights, we increase the scattering strength ratio to some value close to the Ioffe-Regel criterion defined by $kl < 1$ so that localization of light is anticipated.[23,24] For $\lambda/l \sim 1$, with a small imaginary part added to the dielectric constant of the scatterer to model possible absorption effects, we observe extremely localized light-wave pattern, as shown in Fig. 3. The simulation is performed for media of the same size as in Fig. 1, but for clarity we show only the upper part of the region because most light in the strong localized state concentrates within this region. As the number of scatterers is increased, the probability of light paths connected by them to form cycles increases as well. Due to the time reversal symmetry of light propagation, paths having the same cycles but propagating in the opposite direction interfere constructively with the original circular paths, giving rise to strongly localized concentration of light intensities. In fact, as strong-scattering regime is approached, the system exhibits a transition similar to that typically seen

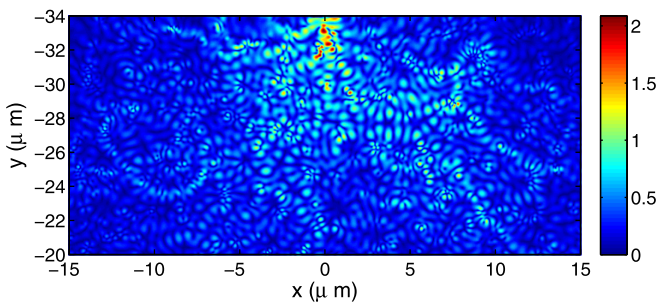

FIG. 3. Emergence of localization of light as the number of disorders is increased to $N = 2000$. Other parameters are the same as in Fig. 1.

in an electronic system, which is transformed from a conducting to an insulating (localized) state.

III. EMERGENCE OF BRANCHED WAVES AND THEIR SCALING BEHAVIOR: THEORY

The problem setting is wave propagation in a two-dimensional optical medium with randomly positioned scattering centers. The material is assumed to be isotropic and *linear*, it is neither dispersive nor dissipative, and there is no source (free charge or current). For disorders with centrosymmetric refractive index distribution, the propagating direction of light wave with linear polarization is confined within a two-dimensional plane.[13] To be concrete, we focus on the TE mode, for which the magnetic field strength is given by $\mathbf{H} = H\mathbf{e}_z$. The Maxwell's equations for $\mathbf{H}$ lead to

$$\nabla \times \left(\frac{1}{\varepsilon}\nabla \times \mathbf{H}\right) = k^2\mu\mathbf{H}, \tag{2}$$

where $k = \omega/c$ is the vacuum wave vector and ε and μ are the relative permittivity and permeability, respectively. The refractive index is $n_0 = \sqrt{\varepsilon\mu}$. For polarized light, Eq. (2) becomes the following Helmholtz equation for the scalar field H:

$$(\nabla^2 + k^2n^2)H = \frac{\nabla n}{n} \cdot \nabla H. \tag{3}$$

The goal of our theoretical analysis is to calculate the scattering field and its statistical distribution throughout the medium. Our approach is to first analyze the field from a single scatterer and then extend the result to multiple scatterers to obtain the statistical properties of the resulted wave intensity. We assume that the random scatterers are far away from each other as compared with their sizes, which can be ensured if they are sparsely distributed in the medium. The shape of the random scatterers will also be taken into account in the analysis.

A. Scattering wave field from a single scatterer

Consider a single scatterer located at the origin. Without loss of generality, we set $n_0 = 1$. For the single-scatterer system we use approximated Gaussian shaped disorders as in our numerical computation, but analysis indicates that the shape of the disorder does not have a significant impact on the statistical properties of the wave intensity distribution.

To proceed, we decompose the magnetic field H into an incident and a scattering part, i.e., $H = H^i + H^s$. The incident field is a plane wave $H^i = e^{ikx}$, whereas the scattering part is the response of the small scatterer to the incident plane wave. If n_0 were not unity, the plane wave should be e^{ikn_0x} instead. For field far away from the scatterer, i.e., $r \gg \sigma$, Eq. (3) becomes

$$(\nabla^2 + k^2)H^s(\mathbf{r}) = f_1 + f_2 + f_3, \tag{4}$$

where

$$f_1(\mathbf{r}) = -(\nabla^2 + k^2 n^2) H^i,$$
$$f_2(\mathbf{r}) = \nabla H^i \cdot \nabla n/n,$$
$$f_3(\mathbf{r}) = \nabla H^s \cdot \nabla n/n.$$

At far field where $H^i \gg H^s$ is satisfied, only f_1 and f_2 contribute to the lowest-order approximation. In particular, to this order, both f_1 and f_2 contain $r^{-1/2}$ term at far field of H^s, whereas f_3 has r^{-1} term. It is thus reasonable to consider contributions from f_1 and f_2 only. Higher-order corrections due to the source term f_3 can be obtained by using recursive iterations, but their contributions to the wave field are insignificant and thus will not be included in our analysis. The Green's function associated with Eq. (4) is

$$(\nabla^2 + k^2) G(\mathbf{r}, \mathbf{r}') = -\delta(\mathbf{r} - \mathbf{r}').$$

The standard solution to the Green's function in two dimensions is given by

$$G(\mathbf{r}, \mathbf{r}') = \frac{i}{4} h_0^{(1)}(k|\mathbf{r} - \mathbf{r}'|),$$

where $h_0^{(1)} = J_0 + iY_0$ is the Hankel function of the first kind. The scattering field can then be written as the summation of two convolution operations

$$H^s(\mathbf{r})_{r \gg \sigma} \approx \sum_{j=1,2} (G * f_j)(\mathbf{r}),$$

where $H_j^s(\mathbf{r}) = (G * f_j)(\mathbf{r})$, $(j = 1, 2)$. Physically, the two scattering fields H_1^s and H_2^s result from the inhomogeneity $n(\mathbf{r})$ in the refractive-index profile and its spatial variations $\nabla n(\mathbf{r})$, respectively, as shown in Fig. 4.

The scattering fields due to f_1 and f_2 can be calculated separately. For example, in order to obtain H_1^s analytically, we approximate the refractive index of the scatterer as

$$n^2(\mathbf{r}) \approx \begin{cases} (1+\Delta n)^2 - \Delta n(1+\Delta n)\left(\dfrac{r}{\alpha\sigma}\right)^2, & r \le r_b, \\ 1, & r > r_b, \end{cases} \quad (5)$$

where

$$r_b = \alpha\sigma\sqrt{\frac{\Delta n + 2}{\Delta n + 1}}$$

is the truncated boundary of the scatterer and α is the parameter that controls the width of variation in n^2, as shown in Fig. 4(a). This form of the refractive index function with a finite domain of disorder profile allows us to evaluate analytically the scattering field at far field by integrating the convolution, which requires the asymptotic form of the Hankel function at far field

$$h_0^{(1)}\left(x \gg \frac{1}{4}\right) \sim \left(\frac{\pi x}{2}\right)^{-1/2} \exp\left(i\left[x - \frac{\pi}{4}\right]\right).$$

The integration is confined within the circle in Fig. 5, i.e., $D(\mathbf{r}') : |\mathbf{r}'| < r_b$. The conditions to ensure the validity of the far-field approximation $x = k|\mathbf{r} - \mathbf{r}'| \gg 1/4$ can be estimated, as follows. For $\Delta n = -0.5$, $\lambda = 1\,\mu$m, $\sigma = 0.22$, and $\alpha = 1$, we have $r_b \approx 0.38\,\mu$m, and $r > 2[10 \cdot (1/4)/k + r_b] \approx 1.56\,\mu$m. This means that, in a $35\,\mu\text{m} \times 70\,\mu\text{m}$ medium, we can have up to 1000 scatterers while still maintaining the sparsity condition, provided that the scatterers are arranged on a lattice. Since, in our simulation, the scatterers are randomly placed in the medium, the acceptable maximum number is considerably less. Using the asymptotic form of the Hankel function, the field $H_1^s(\mathbf{r})$ becomes

$$\begin{aligned} H_1^s(\mathbf{r})_{r \gg r_b} &= \iint_{D(\mathbf{r}')} d\mathbf{r}'\, G(\mathbf{r}, \mathbf{r}') f_1(\mathbf{r}') \\ &= \iint_{D(\mathbf{r}')} d\mathbf{r}'\, \frac{i}{4} h_0^{(1)}(k|\mathbf{r} - \mathbf{r}'|)(-\nabla'^2 - k^2 n^2)\, e^{ikx'} \\ &\approx \frac{i}{4}\sqrt{\frac{2}{\pi}} e^{-i\frac{\pi}{4}} k^{3/2} \cdot \Delta n \left[\frac{(\Delta n + 1)}{\sigma^2} I_1^{(2)} - (\Delta n + 2) I_1^{(0)}\right], \end{aligned}$$

where the integrals $I_1^{(\ell)}(\mathbf{r})$ of orders $\ell = 0, 2$ are of the following form:

$$I_1^{(\ell)}(\mathbf{r}) = \iint_{|\mathbf{r}'| < r_b} d\mathbf{r}'\, r'^{\ell}\, \frac{e^{ik(|\mathbf{r} - \mathbf{r}'| + x')}}{\sqrt{|\mathbf{r} - \mathbf{r}'|}}.$$

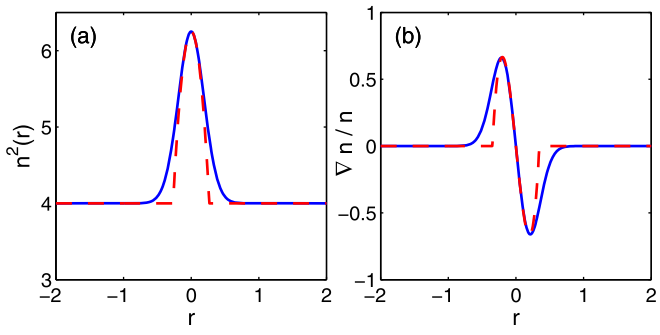

FIG. 4. Approximations of (a) n^2 and (b) $\nabla n/n$ as functions of the distance from center of the scatter. Blue solid lines represent the refractive-index profiles of the Gaussian-shaped scatterer, and the red dashed lines are the polynomial approximations. The typical parameters shown here are $n_0 = 2$, $\Delta n = 0.5, \sigma = 0.2\mu$m, $\alpha = 1$, and $\beta = 2/3$.

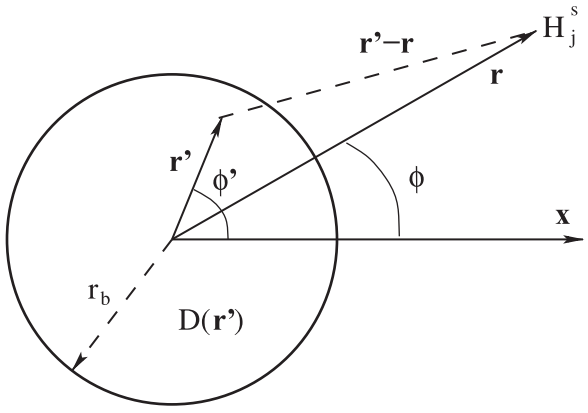

FIG. 5. Integration domain $D(\mathbf{r}')$ of a single scatterer located at the origin with a truncated radius r_b. The incident beam is from $-x$ direction and the scattered field H_j^s is evaluated at far field $\mathbf{r}$.

Similarly, for $H_2^s(\mathbf{r})$ resulting from the source term f_2, we expand $\nabla n/n$ as

$$\frac{\nabla n}{n} \approx \begin{cases} \dfrac{\Delta n}{1+\Delta n}\left(1-\dfrac{\beta r^2}{2\sigma^2}\right)\left(-\dfrac{\mathbf{r}}{\sigma^2}\right), & r \le r_b', \\ 0, & r > r_b', \end{cases} \tag{6}$$

where

$$r_b' = \sigma\sqrt{\frac{2}{\beta}}.$$

An approximate form of $\nabla n/n$ is shown in Fig. 4(b), where we use matched values of α and β so that the boundaries are identical for both integration domains, i.e., $r_b = r_b'$. Under these approximations, H_2^s can be written as

$$H_2^s(\mathbf{r})_{r\gg r_b'} \approx -\frac{1}{4}\sqrt{\frac{2}{\pi}}e^{-i\frac{\pi}{4}}k^{1/2}\cdot\frac{\Delta n}{(1+\Delta n)\sigma^2}\left[\frac{\beta}{2\sigma^2}I_2^{(2)} - I_2^{(0)}\right],$$

where the integrals $I_2^{(\ell)}$ for orders $\ell = 0, 2$ are defined to be

$$I_2^{(\ell)}(\mathbf{r}) = \iint\limits_{|\mathbf{r}'|<r_b'} d\mathbf{r}'\, r'^{\ell}\, x'\, \frac{e^{ik(|\mathbf{r}-\mathbf{r}'|+x')}}{\sqrt{|\mathbf{r}-\mathbf{r}'|}}.$$

To calculate $I_j^{(\ell)}$'s, we use polar coordinates, as depicted in Fig. 5. In the region $r \gg r_b$, the approximations

$$|\mathbf{r}-\mathbf{r}'| \approx r - \hat{\mathbf{r}}\cdot\mathbf{r}' = r - r'\cos(\phi-\phi')$$

and

$$\frac{1}{\sqrt{|\mathbf{r}-\mathbf{r}'|}} \approx r^{-1/2}\left[1+\frac{1}{2}\frac{r'}{r}\cos(\phi-\phi')\right]$$

hold, where $\hat{\mathbf{r}}$ is the unit vector in the direction of $\mathbf{r}'$, ϕ and ϕ' (cf., Fig. 5) are the polar angles of $\mathbf{r}$ and $\mathbf{r}'$, respectively. It can be shown that all the integrals involved in the two scattering fields have the general form

$$\begin{aligned} I_{\tau\mu\nu}(r,\phi) = &\int_0^R dr' \int_0^{2\pi} d\phi'\, r'^{\tau}\cos^{\mu}\phi'\cos^{\nu}(\phi-\phi') \\ &\times\exp(ikr'[\cos\phi' - \cos(\phi-\phi')]), \end{aligned} \tag{7}$$

where R denotes r_b or r_b', and $\tau, \mu, \nu \in \mathbb{N}$. More specifically, $I_j^{(\ell)}$ can be expressed using $I_{\tau\mu\nu}$'s

$$\begin{aligned} I_1^{(0)} &= e^{ikr}\left[r^{-1/2}I_{100} + \frac{1}{2}r^{-3/2}I_{201}\right], \\ I_1^{(2)} &= e^{ikr}\left[r^{-1/2}I_{300} + \frac{1}{2}r^{-3/2}I_{401}\right], \\ I_2^{(0)} &= e^{ikr}\left[r^{-1/2}I_{210} + \frac{1}{2}r^{-3/2}I_{311}\right], \\ I_2^{(2)} &= e^{ikr}\left[r^{-1/2}I_{410} + \frac{1}{2}r^{-3/2}I_{511}\right]. \end{aligned} \tag{8}$$

A key step in obtaining the scattering field is then to integrate $I_{\tau\mu\nu}(r,\phi)$. Take I_{201} for example. We first integrate the ϕ' part by expressing the exponent as

$$\cos\phi' - \cos(\phi-\phi') = \sqrt{2-2\cos\phi}\,\sin(\theta-\phi'),$$

where

$$\sin\theta \equiv \frac{1-\cos\phi}{\sqrt{2-2\cos\phi}}, \quad \text{and} \quad \cos\theta \equiv \frac{\sin\phi}{\sqrt{2-2\cos\phi}}.$$

The integral I_{201} then becomes

$$\begin{aligned} I_{201}(r,\phi) &= \int_0^{r_b} dr' r'^2 \int_0^{2\pi} d\phi'\cos(\phi-\phi') \\ &\quad\times\exp[ikr'\sqrt{2-2\cos\phi}\,\sin(\theta-\phi')] \\ &= 2\pi i\sin(\phi-\theta) \\ &\quad\times\int_0^{r_b} dr' r'^2 J_0'(kr'\sqrt{2-2\cos\phi}) \\ &= -2\pi i\sin(\phi-\theta)\frac{r_b^2 J_2(kr_b\sqrt{2-2\cos\phi})}{k\sqrt{2-2\cos\phi}} \\ &= -\pi i k^{-1} r_b^2 J_2(kr_b\sqrt{2-2\cos\phi}), \end{aligned}$$

where in the last step, we have used $\sin(\phi-\theta) = \sqrt{2-2\cos\phi}/2$. All the integrals are Bessel functions, or more generally, hypergeometric functions. After evaluating all $I_{\tau\mu\nu}$ integrals, we obtain the final scattering fields as

$$\begin{aligned} H_1^s(r,\phi)_{r\gg r_b} &= a_{11}\frac{e^{ikr}}{r^{1/2}}\Phi_1(\phi) + a_{12}\frac{e^{ikr}}{r^{3/2}}\Psi_1(\phi), \\ H_2^s(r,\phi)_{r\gg r_b} &= a_{21}\frac{e^{ikr}}{r^{1/2}}\Phi_2(\phi) + a_{22}\frac{e^{ikr}}{r^{3/2}}\Psi_2(\phi), \end{aligned} \tag{9}$$

where the angular functions are

$$\begin{aligned} \Phi_1(\phi) &= \frac{J_2(kr_b\sqrt{2-2\cos\phi})}{2-2\cos\phi}, \\ \Psi_1(\phi) &= \frac{J_3(kr_b\sqrt{2-2\cos\phi})}{\sqrt{2-2\cos\phi}}, \\ \Phi_2(\phi) &= \frac{J_3(kr_b'\sqrt{2-2\cos\phi})}{\sqrt{2-2\cos\phi}}, \\ \Psi_2(\phi) &= \frac{J_4(kr_b'\sqrt{2-2\cos\phi})}{2-2\cos\phi}, \end{aligned} \tag{10}$$

and the coefficients a_{ij}'s are given by

$$\begin{aligned} a_{11} &= -4\pi k^{-1/2}\left(\frac{i}{4}\sqrt{\frac{2}{\pi}}e^{-i\frac{\pi}{4}}\right)\frac{\Delta n(\Delta n+1)r_b^2}{\sigma^2}, \\ a_{12} &= \pi i k^{-1/2}\left(\frac{i}{4}\sqrt{\frac{2}{\pi}}e^{-i\frac{\pi}{4}}\right)\frac{\Delta n(\Delta n+1)r_b^3}{\sigma^2}, \\ a_{21} &= 2\pi k^{-3/2}\left(\frac{i}{4}\sqrt{\frac{2}{\pi}}e^{-i\frac{\pi}{4}}\right)\frac{\Delta n r_b'}{(\Delta n+1)\sigma^2}, \\ a_{22} &= -\pi i k^{-3/2}\left(\frac{i}{4}\sqrt{\frac{2}{\pi}}e^{-i\frac{\pi}{4}}\right)\frac{\Delta n r_b'^2}{(\Delta n+1)\sigma^2}. \end{aligned} \tag{11}$$

By considering only the lowest order $r^{-1/2}$, we can write the scattering field in the form

$$H^s(r,\phi)_{r\gg r_b,r_b'} = \frac{e^{ikr}}{r^{1/2}}\Phi(\phi), \tag{12}$$

where $\Phi(\phi) = a_{11}\Phi_1(\phi) + a_{21}\Phi_2(\phi)$. While Eq. (12) is derived under the assumption $n_0 = 1$, the cases where n_0 is not unity can be treated by using the simple substitutions $k \to kn_0$ and $\Delta n \to \Delta n/n_0$.

Figures 6(a) and 6(b) show the behavior of the angular part $\Phi(\phi)$ for two distinct cases, corresponding to extreme cases of small and large scatterer-wavelength ratios, respectively. When the ratio r_b/λ is small [Fig. 6(a)], the scattering field is nearly uniform in all directions from the scatterer. In contrast, as the size of the scatterer is increased so that r_b/λ becomes large, the energy associated with the incident wave concentrates mostly in the incident direction, leaving oscillating fields of small amplitude in other directions, as shown in Fig. 6(b). The inset of Fig. 6(b) indicates the oscillatory behavior of the scattering field, which represents the branched but somewhat weak wave flow patterns in different directions. An optimal ratio r_b/λ can be found in between the two cases shown in Fig. 6, implying that the branched structure emerges only when the size of the scatterer is comparable to the incident wavelength.

The scattering field structure calculated directly from Eq. (9) is shown in Fig. 7. In the forward $(+x)$ direction, the strength of the scattering field decreases with the radius and the field is composed of a series of magnified flows radiating in all directions. This faithfully reproduces the typical behavior of the scattering field obtained from direct FDFD simulation where the main wave branches fork into smaller ones when encountering refractive index disorders. Note that in Figs. 7(e) and 7(f), both the $r^{-1/2}$ and $r^{-3/2}$ terms have been taken into account, but the $r^{-3/2}$ term is significantly weaker than the $r^{-1/2}$ term in magnitude [as evidenced in Figs. 7(a)–7(d)], providing further validation of Eq. (12).

Our expression for the scattering field of a single scatterer provides qualitative explanation as to why a highly non-uniform structure associated with the field can arise. In particular, the analytic result explains, instead of a uniform spread of the scattering field in all directions, it tends to form

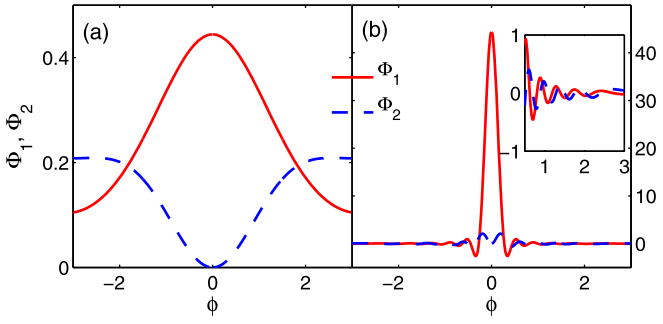

FIG. 6. Angular distributions of the scattering field $H^s(r = const., \phi)$ for two different scatterer-wavelength ratios (r_b/λ). Assuming $r_b = r_b'$, we compute the angular functions Φ_1 and Φ_2 corresponding to scattered fields of order $r^{-1/2}$ under two cases: (a) $r_b/\lambda = 0.3$ and (b) $r_b/\lambda = 3$. The inset of (b) shows the oscillating behavior for $\phi > 0.5$.

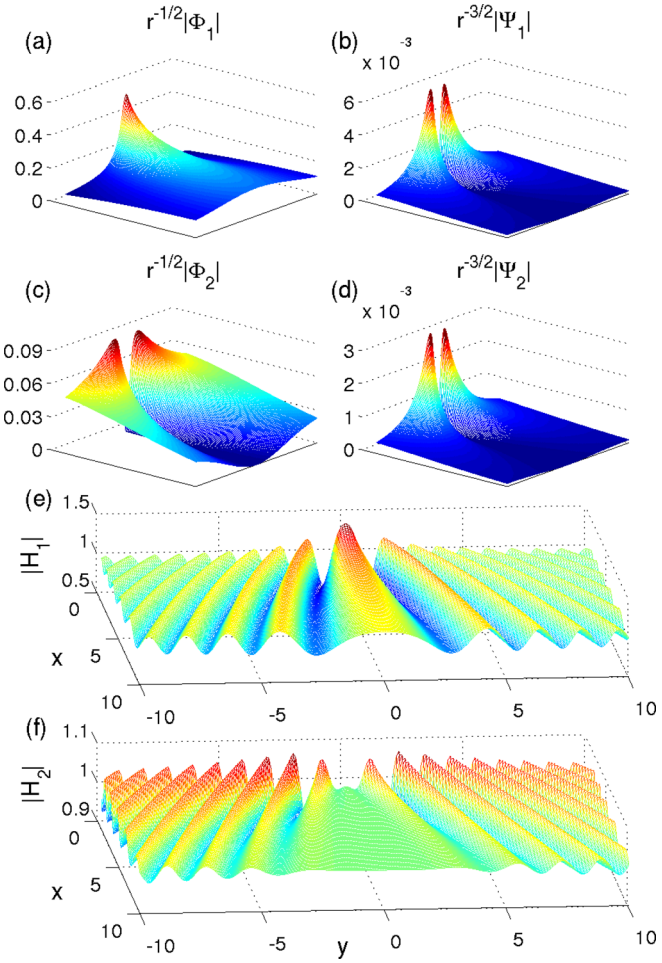

FIG. 7. Forward $(+x)$ scattering fields. Panels (a) and (c) show the magnitude of forward scattering fields of order $r^{-1/2}$ from the source term f_1 in Eq. (4), while panels (b) and (d) show the field magnitude of order $r^{-3/2}$ from the source term f_2, which are much smaller at far field. The total field magnitude $|H_1|$ and $|H_2|$ from two source terms are shown in (e) and (f), respectively. The incident wave (of wavelength $\lambda = 1\mu$m) is sent in the $+x$ direction on a scatterer located at the origin. The parameters characterizing the refractive-index function of the scatterer are $\sigma = 0.22\mu$m and $\Delta n = -0.5$.

a branched structure with hot spots. In the presence of multiple scatterers, each scattering event gives rise to a few dominant branches that spread out to far field. Some of the remaining scatterers are located within the large branches while most other scatterers are located outside any large branched structure. These latter groups of scatterers are essentially not affected by the scattering field. Second-stage scattering will also induce some large branches, which can possibly "meet" with the branches from the first-stage scattering and generate constructive interference. Highly localized structure of the field can result from such interference. The probabilities of destructive and constructive interferences are approximately the same. However, since the higher-level scattering fields are necessarily weaker than the ancestor wave branches, the already generated intense branches cannot be eliminated, especially for the branches near the center direction of the propagation. This provides a plausible explanation as to why in most cases the strongest branch in our simulation either is along the center direction or titles slightly to one side. The former is due to equal

probabilities that the random scatterers appear on both sides of the main propagation direction, and the latter is caused by the asymmetric distribution of the refractive index of the scatterer on both sides. This branch-accumulation process is extremely sensitive to the disorders' spatial distribution, leading to the emergence of branched wave patterns.

B. Multiple disorders

Based on the results from a single scatterer, we now analyze the scattering field due to multiple random scatterers. Although a general analysis of coherent scattering of light in random medium has been available for many years (see, for example, Ref. 22), our focus here is on the emergence and statistical properties of branched waves. To make analysis feasible, we assume that all scatterers have the same size and are relatively far from each other: $r_{ij} \gg r_b$, as shown in Fig. 8, where r_{ij} is the distance between scatterers i and j, and r_b is the size of each scatterer. The scatterers can then be regarded as weakly correlated, rendering applicable our analysis leading to Eq. (12) of the scattering field from a single scatterer. Let i denote the primary scatterer and consider another scatterer, denoted by j. Waves scattered from i can undergo a secondary scattering process off scatterer j. Let the original incident wave direction be $+x$ and the direction from i to j be $+x\prime$. The primary scattering field is the incident wave of secondary scattering off scatterer j. The transformation from frame ($x\prime$, $y\prime$) to frame (x,y) is

$$\mathbf{r} = \mathbf{R}(\phi_j)\mathbf{r}' + \mathbf{r}_{ij},$$

where $\mathbf{R}(\phi_j) = \begin{pmatrix} \cos\phi_j & -\sin\phi_j \\ \sin\phi_j & \cos\phi_j \end{pmatrix}$ is the rotation operator. According to Eq. (12), we write the scattering field from scatterer i in the vicinity of scatterer j as

$$\frac{e^{ik|Rr'+\mathbf{r}_{ij}|}}{\sqrt{|Rr'+\mathbf{r}_{ij}|}}\Phi(\phi) \approx \frac{e^{ikr_{ij}}e^{ikr'\cos\phi'}}{\sqrt{r_{ij}+r'\cos\phi'}}\Phi(\phi_j) \approx \frac{e^{ikr_{ij}}}{\sqrt{r_{ij}}}\Phi(\phi_j)e^{ikx'}.$$

Since the $e^{ikx'}$ term is now the incident plane wave for the secondary scattering process, to the lowest order $r^{-1/2}$, the scattering fields from the first and second stages differ by only a fixed pattern factor. To define this factor properly, we consider three scatterers (denoted by i,j,ℓ) through which the light passes successively, forming a multiple scattering process. The cumulative factor can then be defined as

$$q_{i,j,\ell} = \frac{e^{ik|\mathbf{r_j}-\mathbf{r_i}|}}{\sqrt{|\mathbf{r_j}-\mathbf{r_i}|}}\Phi[\arccos(\mathbf{e}_{ij}\cdot\mathbf{e}_{j\ell})],$$

where $\mathbf{e}_{ij}$ is the unit vector in the direction of $\mathbf{r}_j - \mathbf{r}_i$.

Let the subscript 0 denote infinity where the incident wave is originated and assume that the incident wave beam is first scattered by only one scatterer, labeled by 1. Treating the field point j as another scatterer, we obtain the total field from all possible scattering paths

$$q_{0,1,j} + \sum_i q_{0,1,i}q_{1,i,j} + \sum_{i,\ell} q_{0,1,i}q_{1,i,\ell}q_{i,\ell,j} + \cdots. \tag{13}$$

If the scatterers are randomly distributed, the summation over the same scattering level will not cause order-of-magnitude changes in the scattering field, due to the fact that complex variables of similar magnitude but of random phases will cancel each other, generating a complex number close to the origin in the complex plane. In order to obtain an analytic expression for the total scattering field so that its statistical properties can be analyzed, we need to make approximations on each $q_{i,j,\ell}$ term. Specifically, we write

$$q_{i,j,\ell} \approx q(\rho,\varphi) = \rho^{-1/2}\exp(ik\rho)\Phi(\varphi),$$

where ρ is the distance between each pair of scatterers and φ is the angle determined by the relative positions of the three consecutive scatterers. Under this approximation, the sum of the first m terms in Eq. (13) becomes

$$S_m = q + q^2 + q^3 + \cdots + q^m.$$

Letting $q = ae^{i\theta}$, where $a \geq 0$, we get the sum of the geometric series $S_\infty = ae^{i\theta}/(1-ae^{i\theta})$. Similar to geometric series of real numbers, $a \in [0,1)$ is the condition that guarantees the convergence of the sum. In our case, this condition is satisfied because we assume weakly correlated scatterers so that $a \to 0$. The total intensity of the scattering field is then

$$I(\rho,\varphi) = |S_\infty|^2 = \left|\frac{ae^{i\theta}}{1-ae^{i\theta}}\right|^2.$$

Under the assumption that $a \to 0$, the intensity can be written as

$$I = \left|\frac{ae^{i\theta}-a^2}{1-2a\cos\theta+a^2}\right|^2 \approx \frac{a^2}{1-4a\cos\theta} \approx a^2 + 4a^3\cos\theta.$$

To the lowest order, the intensity can be expressed in the following simple form:

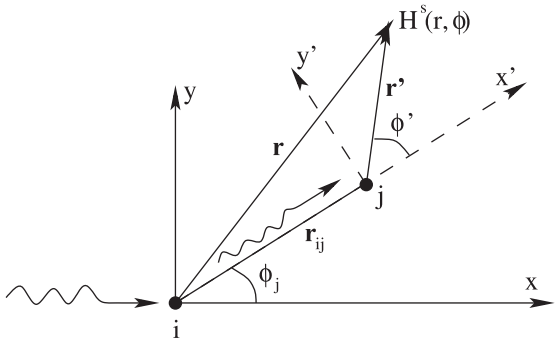

FIG. 8. Multiple scattering from two scatterers, labeled as i and j and separated by distance $|\mathbf{r}_{ij}|$. In the case of well-separated scatterers, the final scattering field can be interpreted as a cumulative scattering process by multiple scatterers, with each individual scattering event being analogous to the scattering of a single disorder.

$$I = \frac{|\Phi(\varphi)|^2}{\rho}, \tag{14}$$

which is similar to that in the case of a single scatterer. This is reasonable because, under the assumption of weakly correlated scatterers, contributions from higher-level scattering processes are negligibly small.

C. Scaling laws for intensity distribution

The probability distribution of the intensity of the scattering field can be obtained if the distributions of the position parameters ρ and φ are available. To be concrete, denote $f_{\rho,\varphi}(\rho,\varphi)$ as the joint probability density function (PDF) of random variables ρ and φ. The expression $I = I(\rho,\varphi)$ alone is not sufficient to derive the PDF of the intensity. What is needed is an auxiliary function $J = J(\rho,\varphi)$. We have

$$f_I(I) = \int f_{I,J}(I,J)dJ = \int \frac{f_{\rho,\varphi}(\rho(I,J),\varphi(I,J))}{\left|\det\left(\frac{\partial(I,J)}{\partial(\rho,\varphi)}\right)\right|}dJ, \tag{15}$$

where $\frac{\partial(I,J)}{\partial(\rho,\varphi)}$ is the Jacobian matrix associated with the corresponding transformation. The joint PDF of the variables in the polar coordinate is proportional to the unit area of the two-dimensional plane, $f_{\rho,\varphi} \sim \rho$, and a proper choice for $J(\rho,\varphi)$ is $J = \varphi$. We then obtain the following algebraic scaling law of the PDF with respect to the intensity of the scattering field:

$$f_I(I) \propto I^{-\gamma}, \tag{16}$$

where $\gamma = 3$ for our minimal model.

To verify the algebraic scaling law, we carry out extensive FDFD computations for different realizations of random scatterers of different densities, which are uniformly distributed within a 35 μm × 70 μm rectangular dielectric medium. Figure 9 presents a case where there are 300 random scatterers in the region, as illustrated in (a). A pronounced branched wave pattern is observed, as shown in Fig. 9(b). Figure 9(c) shows, on a logarithmic scale, the corresponding intensity distribution. We observe that, for intensity up to a reasonably high value, the distribution is power-law, as predicted by our theory. The power-law exponent, however, is slightly less than the theoretically predicted value –3. The main reason is that the theoretical scaling law I^{-3} is derived under the assumption of sparse scatterers. When there are 300 scatterers in the 35 μm × 70 μm rectangular scattering region, the average distance between any pair of scatterers is not significantly larger than the wavelength (1 μm), so the condition of sparse scatterers may not have been met (as we will show below in another example, when the scatterers are sparser, the agreement with theory is improved markedly). From the inset in Fig. 9(c) where the intensity distribution is plotted on a logarithmic-linear scale, we observe an exponential tail (or cut-off) in the very high intensity regime. The main reason is lack of sufficient statistics at extremely high intensity. Another plausible reason is random speckle fields. We note that the issue of insufficient number of extreme statistical

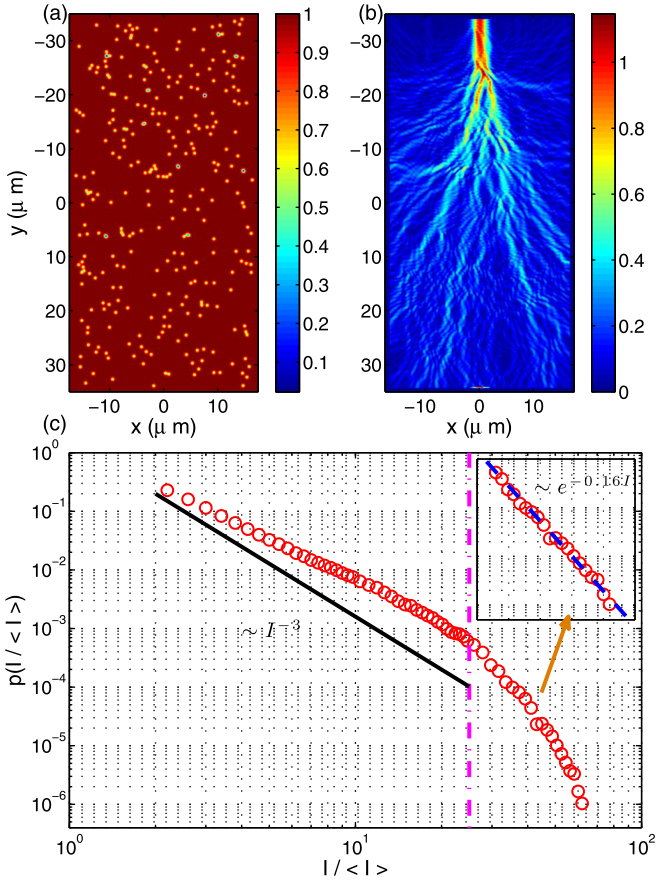

FIG. 9. (a) Distribution of 300 random scatterers in a 35μm × 70μm uniform medium. (b) Branched wave magnitude from FDFD simulation. The incident wave is uniform with width λ and sent in the $+y$ direction, where $\lambda = 1\mu$m, $n_0 = 1, \Delta n = -0.5$, and $\sigma = 0.22\mu$m. (c) Numerically obtained scaling law of the intensity distribution (blue circles) and the theoretical prediction (black solid line $\sim I^{-3}$) on a logarithmic scale. The scaling behavior is mostly power-law but has an exponential tail in the high-intensity regime, as shown on a logarithmic-linear scale in the inset of (c). The numerically obtained power-law exponent is slightly less than the theoretically predicted value −3.

events is common for any realistic situation of power-law fit, as the computation can be done only to a finite extent. In our case, the scattering domain is only reasonably large due to the limitation of our computational resource, which artificially reduces the probability for extremely high intensity events to occur.

As the scatterer distribution becomes sparser, we expect the power-law scaling exponent to be closer to the theoretical value –3. One example is shown in Fig. 10(a), where there are now only 50 random scatterers in the same rectangular region as in Fig. 9(a). The observed scattering wave field still has a pronounced branched structure, as shown in Fig. 10(b). The intensity distribution follows a power-law, as shown on a logarithmic scale in Fig. 10(c), but the scaling exponent is now much closer to the theoretical value. Similar to Fig. 9(c), there is an exponential cut-off at extremely high intensity values, as shown in the inset of Fig. 10(c). The critical intensity value at which the exponential behavior starts is somewhat smaller than the case in Fig. 9(c). This can be qualitatively understood by noting that when the random scatterers are weakly correlated, the intensity distribution follows a power-law, implying the existence of "hot" branches with extremely

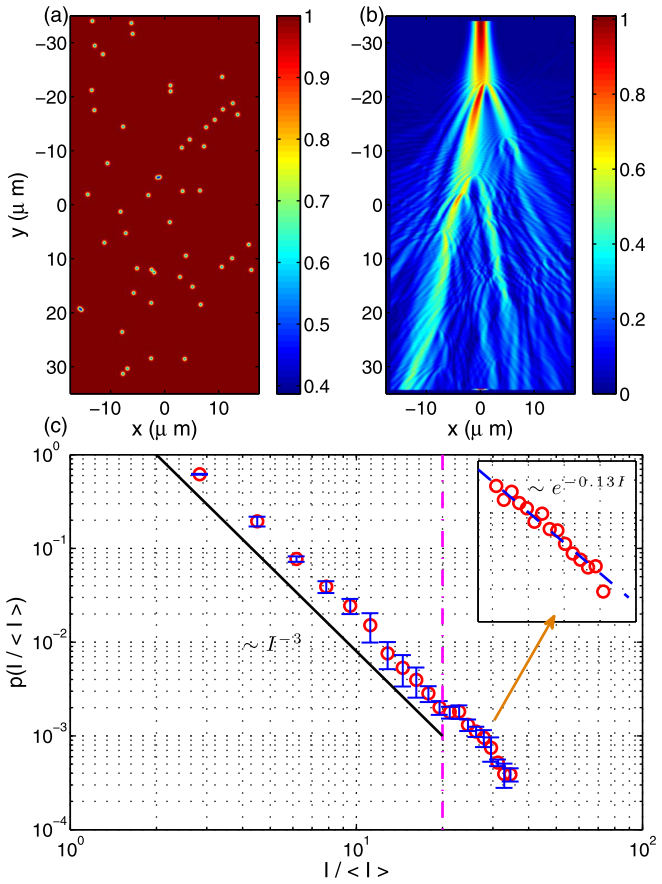

FIG. 10. (a) Distribution of 50 random scatterers in the 35μm $\times$ 70μm uniform medium. (b) Branched wave magnitude from FDFD simulation. The incident wave is uniform with width λ and sent in the $+y$ direction, where $\lambda = 1\mu$m, $n_0 = 1$, $\Delta n = -0.5$, and $\sigma = 0.23\mu$m. (c) Numerically obtained scaling law of the intensity distribution (blue circles) on a logarithmic scale and the theoretical prediction (solid line $\sim I^{-3}$). There is an exponential cutoff in the high-intensity regime, as shown in the inset.

high local intensities. As the density of the random scatterers is decreased, this hallmark of branched waves tends to be somewhat weakened because, when the scatterers are further apart, the intensity of the wave scattered from one scatterer may already have weakened significantly before reaching the next scatterer, making it less probable for fields from different levels of scattering to interfere constructively.

D. Effect of shape of random scatterer

Our theoretical analysis and numerical simulations indicate that the shape of the random scatterer has little effect on the scaling law associated with the intensity of the branched wave patterns. The shape, however, can affect the weight of each of the r^n term as well as the weights of the H_1^s and H_2^s terms in, for example, the scattering fields in Fig. 7. Because the total scattering field is the sum of all terms, a change in the shape of the scatterer can induce a change in the pattern of the scattering fields. But if the scatterers are sparse in the medium, the effect can still be quite small. Additional insights can be obtained by examining the process leading to the scattering intensity given by Eq. (14). When we perform the integration to obtain the PDF of intensity, the polar angle ϕ part only contributes to the normalization constant while the exponent value –3 remains unchanged. This treatment is valid for the lowest-order approximation of intensity, in which the scatterer shape can only affect the angular ϕ part and therefore will not affect the field intensity distribution. When high-order terms are included, the polar angle may become important, in which case the shape of the scatter can affect the algebraic scaling exponent in the branched wave intensity distribution.

IV. CONCLUSIONS AND DISCUSSIONS

Extreme wave phenomena were historically documented in oceanography. Recent experimental efforts have demonstrated, however, that they can occur in a wide variety of physical systems such as two-dimensional electron gas, superfluid Helium, microwave systems, optical fibers, and optical cavities. Despite the intense efforts, the physical origin of branched waves remains to be elusive and an actively debated issue. For example, earlier it had been thought that nonlinearity, or weak nonlinearity, should be a necessary condition for branched waves, but very recent experiments demonstrated that even linear medium can generate these waves.[8,12] It seems from all previous works, though, that random wave scattering is a necessary condition for the emergence of branched waves. In many experiments, significant deviations of the light intensity from the Gaussian distribution were observed. In fact, a characteristic feature of branched waves is the "long-tail" distribution in their intensities, leading to localized regions in the space with significantly higher intensity than those in the rest. A paradigmatic model that contains absolutely the minimal physical ingredients necessary for branched waves is needed to understand the origin of these exotic waves.

We have analyzed a minimal model that we recently proposed to explain the emergence of branched waves. The model contains two essential ingredients: (1) a finite medium for linear wave propagation and (2) random scatterers in the medium whose physical properties deviate from those of the background medium. To facilitate computation and theoretical analysis, we have considered wave systems in two dimensions. For numerical simulations we assume a generic form of the refractive-index distribution function for each scatterer. For analytic treatment, we have used an approximate form of the index function. In both cases, robust branched wave patterns in a wide range of system parameters with algebraic (power-law) tails in the distribution of the wave intensity have been observed or predicted, indicating that branched waves are a general phenomenon, regardless of the difference in the physical properties of the random scatterers. Our detailed analysis suggests that the origin of branched waves can be attributed to two basic phenomena: (1) break-up of wave by a single scatterer and (2) constructive interference of "broken waves" by multiple scatterers randomly located in the space. Note that these two phenomena are fairly "elementary" in wave physics, and we believe that they explain why branched waves should be a universal phenomenon in all kinds of wave systems. Although our computations and analysis are for optical waves, the physical insights should be applicable to many other wave systems in various areas of science and engineering.

In electromagnetics, coherent multiple scattering of light through random media was studied extensively in the past,[22,25,26] although these studies were not directly pointed at the phenomenon of branched wave structures. A related phenomenon is Anderson localization of light in random media. In particular, a basic theory in the scattering of electromagnetic waves in random media is the scaling theory of localization,[27] where the scattering strength, characterized by the ratio of wavelength λ and the math free path l, increases as l decreases. In the classical limit where $\lambda/l \ll 1$, phase correlation is weak so that the approximation of self-avoiding multiple scattering can be used. However, in the strong scattering limit, constructive and destructive wave interferences become dominant. In this case, one has $\lambda \sim l$, and the phenomenon of light localization emerges, similar to the phenomenon of Anderson localization in condensed matter physics.[28] In fact, Anderson localization of light was theoretically predicted[23,24] and experimentally confirmed.[29–32]

The study of complex wave patterns in optical media and their underlying physical mechanism can have broader applications. For example, structural disorders are inherent to the fabrication process of many optical devices such as photonic crystals,[33,34] and the occurrence of extremely high intensity wave branches can be detrimental to the device operation due to the random nature of the waves. Even worse, the existence of hot spots of excessive intensities associated with the branched wave structures can cause irreversible damage to the device. On the other hand, since the random, spatially localized disorders that we treat in this paper can have positive or negative refractive constants, our work may be relevant to the extremely active field of optical metamaterials[35,36] and devices. From a different perspective, the possibility that branched waves with hot spots can be induced in realistic optical media implies potential applications in defense, where defeating adversarial systems using electromagnetic waves is of significant interest. Suppose an adversarial system that contains some optical media poses a threat. Inducing branched waves in the media may cause desirable damages to the intended operation of the system.

A final remark is that, the algebraic scaling exponent $\gamma = 3$ in the intensity distribution of branched waves is obtained for Gaussian type of refractive-index distribution function or its approximation for random scatterers. Deviation from the Gaussian shape can cause the scaling exponent to be different. Thus, in general, we do not anticipate to observe the exponent value of 3 associated with branched waves. However, the algebraic scaling relation or the long-tail behavior is generic for branched waves arising in different fields.

ACKNOWLEDGMENTS

This work was supported by AFOSR under Grant No. FA9550-12-1-0095 and by ONR under Grant No. N00014-08-1-0627.

[1]B. S. White, J. Fluid Mech. **355**, 113 (1998); M. Onorato, A. R. Osborne, and M. Serio, Phys. Rev. Lett. **96**, 014503 (2006); N. Akhmediev, J. M. Soto-Crespo, and A. Ankiewicz, Phys. Lett. A **373**, 2137 (2009); B. Eliasson and P. K. Shukla, Phys. Rev. Lett. **105**, 014501 (2010); K. Hammani, B. Kibler, C. Finot, and A. Picozzi, Phys. Lett. A **374**, 3585 (2010).
[2]M. A. Wolfson and S. Tomsovic, J. Acoust. Soc. Am. **109**, 2693 (2001); F. J. Beron-Vera, M. G. Brown, J. A. Colosi, S. Tomsovic, A. L. Virovlyansky, M. A. Wolfson, and G. M. Zaslavsky, *ibid.* **114**, 1226 (2003); M. G. Brown, J. A. Colosi, S. Tomsovic, A. L. Virovlyansky, M. A. Wolfson, and G. M. Zaslavsky, *ibid.* **113**, 2533 (2003).
[3]M. Onorato, T. Waseda, A. Toffoli, L. Cavaleri, O. Gramstad, P. A. E. M. Janssen, T. Kinoshita, J. Monbaliu, N. Mori, A. R. Osborne, M. Serio, C. T. Stansberg, H. Tamura, and K. Trulsen, Phys. Rev. Lett. **102**, 114502 (2009).
[4]D. R. Solli, P. Ropers, C. Koonath, and B. Jalali, Nature (London) **450**, 1054 (2007).
[5]J. M. Dudley, G. Genty, and B. Eggleton, Opt. Express **16**, 3644 (2008).
[6]A. N. Ganshin, V. B. Efimov, G. V. Kolmakov, L. P. Mezhov-Deglin, and P. V. E. McClintock, Phys. Rev. Lett. **101**, 065303 (2008).
[7]A. Montina, U. Bortolozzo, S. Residori, and F. T. Arecchi, Phys. Rev. Lett. **103**, 173901 (2009).
[8]F. T. Arecchi, U. Bortolozzo, A. Montina, and S. Residori, Phys. Rev. Lett. **106**, 153901 (2011).
[9]M. A. Topinka, B. J. LeRoy, R. M. Westervelt, S. E. J. Shaw, R. Fleischmann, E. J. Heller, K. D. Maranowski, and A. C. Gossard, Nature (London) **410**, 183 (2001).
[10]L. Kaplan, Phys. Rev. Lett. **89**, 184103 (2002).
[11]N. Akhmediev and E. Pelinovsky, Eur. Phys. J. Spec. Top. **185**, 1 (2010) and references therein.
[12]R. Höhmann, U. Kuhl, H.-J. Stöckmann, L. Kaplan, and E. J. Heller, Phys. Rev. Lett. **104**, 093901 (2010).
[13]X. Ni, W.-X. Wang, and Y.-C. Lai, Europhys. Lett. **96**, 44002 (2011).
[14]R. C. Rumpf, "Design and optimization of nano-optical elements by coupling fabrication to optical behavior," Ph.D. dissertation (University of Central Florida, 2006).
[15]C.-P. Yu and H.-C. Chang, Opt. Express **12**, 1397 (2004).
[16]S.-D. Wu and E. N. Glytsis, J. Opt. Soc. Am. A **19**, 2018 (2002).
[17]Briefly, this method uses Yee's grid, which is a leap-frog discretization scheme for electric and magnetic field components. Instead of solving the Maxwell curl equations directly with time iterations as in the classical FDTD scheme, FDFD considers a snapshot of the steady state and uses matrix formulation to solve the whole material system at once. See, for example, Refs. 15 and 16.
[18]B. Shapiro, Phys. Rev. Lett. **57**, 2168 (1986).
[19]T. M. Nieuwenhuizen and M. C. W. V. Rossum, Phys. Rev. Lett. **74**, 2674 (1995).
[20]A. D. Mirlin, R. Pnini, and B. Shapiro, Phys. Rev. E **57**, R628 (1998).
[21]M. Störzer, P. Gross, C. M. Aegerter, and G. Maret, Phys. Rev. Lett. **96**, 063904 (2006).
[22]E. Akkermans, P. E. Wolf, and R. Maynard, Phys. Rev. Lett. **56**, 147 (1986).
[23]S. John, Phys. Rev. Lett. **53**, 216 (1984).
[24]S. John, Phys. Rev. B **31**, 30 (1985).
[25]P.-E. Wolf and G. Maret, Phys. Rev. Lett. **55**, 269 (1985).
[26]D. S. Wiersma, M. P. V. Albada, B. A. V. Tiggelen, and A. Lagendijk, Phys. Rev. Lett. **74**, 419 (1995).
[27]E. Abrahams, P. W. Anderson, D. C. Licciardello, and T. V. Ramakrishnan, Phys. Rev. Lett. **42**, 67 (1979).
[28]P. W. Anderson, Phys. Rev. **109**, 1492 (1958).
[29]D. S. Wiersma, P. Bartolini, A. Lagendijk, and R. Righini, Nature Mater. **390**, 671 (1997).
[30]A. A. Chabanov, M. Stoytchev, and A. Z. Genack, Nature (London) **404**, 850 (2000).
[31]T. Schwartz, G. Bartal, S. Fishman, and M. Segev, Nature (London) **446**, 52 (2007).
[32]Y. Lahini, A. Avidan, F. Pozzi, M. Sorel, R. Morandotti, D. N. Christodoulides, and Y. Silberberg, Phys. Rev. Lett. **100**, 013906 (2008).
[33]S. Hughes, L. Ramunno, J. F. Young, and J. E. Sipe, Phys. Rev. Lett. **94**, 033903 (2005).
[34]M. Patterson, S. Hughes, S. Combrié, N.-V.-Q. Tran, A. D. Rossi, R. Gabet, and Y. Jaouën, Phys. Rev. Lett. **102**, 253903 (2009).
[35]N. Engheta, R. W. Ziolkowski, I. O. Electrical, and E. Engineers, *Metamaterials: Physics and Engineering Explorations* (John Wiley & Sons, 2006).
[36]D. Morits and C. Simovski, Phys. Rev. B **82**, 165114 (2010).